Nuclear Science and Techniques (2025) 36:12
https://doi.org/10.1007/s41365-024-01568-1

Polypropylene-based blend with enhanced breakdown strength under gamma-ray irradiation for cable insulation

Bai-Xin Liu[1] · Yu Gao[1] · Jing Li[1] · Chen-Yi Guo[1] · Bo-Sen Si[1] · Jun-Guo Gao[2] · Yu Chen[3] · Bo-Xue Du[1]

Received: 31 January 2024 / Revised: 26 March 2024 / Accepted: 21 April 2024 / Published online: 19 December 2024

Abstract

This study focuses on the electrical properties and microstructure of polypropylene (PP)-based blends used for cable insulation in nuclear power plants (NPPs). The PP-based blend, comprising isotactic PP and propylene-based elastomer (PBE) at concentrations ranging from 0 to 50 wt%, underwent a melt blending process and subsequent cobalt-60 gamma-ray irradiation with doses ranging from 0 to 250 kGy. Electrical conductivity, trap distribution, and alternating (AC) breakdown strength were chosen to assess the insulation performance. These results indicate that the addition of PBE significantly improves the electrical properties of PP under irradiation. For PP, the electrical conductivity increased with irradiation, whereas the trap depth and breakdown strength decreased sharply. Conversely, for the blend, these changes initially exhibit opposite trends. When the irradiation was increased to 250 kGy, the AC breakdown strength of the blend improved by more than 21% compared to that of PP. The physical and chemical structures of the samples were investigated to explore the improvement mechanisms. The results offer insights into the design of new cable-insulation materials suitable for NPPs.

Keywords Nuclear power plant · Cable insulation · Polypropylene · Electrical properties · Gamma-ray irradiation

1 Introduction

Global attention is directed toward nuclear power, as it presents a low-carbon-emission alternative and holds promise for addressing energy crises [1]. In 2023, a high-temperature gas-cooled reactor (HTGCR) nuclear power plant (NPP) commenced commercial operation, showcasing enhanced safety and power generation efficiency [2–4]. Various types of nuclear power cables are crucial to ensure the safe operation of NPPs. The ambient temperature of nuclear power cables operating in HTGCR NPPs is 10–50 °C higher than that of previous NPPs, leading to serious challenges in cable insulation [5]. For polymer materials used in HTGCR NPPs, high-temperature resistance is imperative. The operating temperature range of polyethene (PE), which is the primary material for cable insulation, is constrained by its melting point of 90 °C [6, 7]. Other commonly used polymer materials have also proven challenging for HTGCR NPPs [8]. However, polypropylene (PP), with a melting point exceeding 170 °C, is considered as a promising candidate and is widely recognized as an insulation material owing to its chemical resistance, low density, and excellent electrical properties [9, 10].

Extensive studies have been conducted on the applicability of PP to NPPs. Cygan et al. demonstrated that PP can serve as a dielectric in reactor environments owing to its exceptional electrical properties under neutron radiation [11]. The material exhibited a marginal reduction in breakdown voltage and an increase in dielectric loss following exposure to fast neutrons and gamma radiation for 10 h. The breakdown strength and volume resistivity increased

This work was supported by the National Natural Science Foundation of China (No. 52077151), the State Key Laboratory of Electrical Insulation and Power Equipment (No. EIPE23208), and the Key Laboratory of Engineering Dielectrics and Its Application, Ministry of Education (No. KFM202203).

✉ Yu Gao
hmgaoyu@tju.edu.cn

[1] School of Electrical and Information Engineering, Tianjin University, Tianjin 300072, China

[2] Key Laboratory of Engineering Dielectrics and Its Application, Ministry of Education, Harbin University of Science and Technology, Harbin 150080, China

[3] State Key Laboratory of Electrical Insulation and Power Equipment, Xi'an Jiaotong University, Xi'an 710049, China

owing to the combined neutron-gamma radiation at a dose of 16 kGy [12]. At higher doses, the degradation due to irradiation may affect its suitability. It has been determined that the failure of PP materials during irradiation aging mainly involves chain scission [13, 14]. Hammoud et al. revealed that the electrical properties of PP can withstand exposure to an electron beam with doses up to 100 kGy, but the mechanical properties exhibit degradation even at 10 kGy [15]. This transformation results from a chain scission reaction of the molecules created by irradiation. Yoshiaki et al. observed increased radiation-induced conductivity in PP subjected to combined heat and irradiation conditions [16]. Mouaci et al. reported that gamma-ray irradiation leads to an increase in the conductivity of PP at a dose of 100 kGy, which is the result of oxidation and changes in crystallinity [17]. Based on its excellent electrical performance, the application of PP in NPPs is anticipated; however, its long-term utilization is significantly constrained by irradiation-induced aging, notably chain scission. A comprehensive understanding of the irradiation-induced damage in PP is crucial for enhancing its performance and usage security, necessitating the exploration of microstructural changes.

Numerous studies explored the effects of irradiation on the structural degradation of PP. Wang et al. investigated performance alterations in PP subjected to 1.2 MeV static electron beam irradiation at a dose rate of 20 kGy/h [18]. As cumulative dose increases, both the carbonyl index and free radical concentration increase. There is a simultaneous decrease in the mechanical performance and significant alterations in the melting and crystallization behaviors, which is indicative of the profound impact of irradiation on the structure of PP [19]. Oxana et al. revealed the presence of a substantial number of degraded compounds with diverse structures in PP irradiated with only 20 kGy gamma-rays [20]. It is clear that the structure of PP has a heightened sensitivity to irradiation, which may induce chain scission and oxidation [21]. In PP, a substantial quantity of tertiary carbon within the macrochains is pivotal for chain scission [22]. Even if the initial melting point is high and the electrical performance is excellent, the cumulative damage that may be created is crucial for the safety of its operation in NPPs. Hence, it is important to improve the irradiation resistance of PP to maintain superior electrical properties under long-term irradiation. Surprisingly, research on the irradiation resistance of PP, particularly regarding the enhancement of its electrical performance under irradiation, is scarce. Propylene-based elastomers (PBE) exhibit good compatibility with PP and have been reported to enhance the flexibility and reduce the partial discharge erosion of PP samples [21–25], which is beneficial for the use of PP-based materials as cable insulation. However, research on the effect and mechanism of PBE content on the irradiation resistance of PP-based materials, which is necessary for their use as nuclear cable insulation, has not been conducted.

In this study, PBE was used to enhance the electrical properties of PP under irradiation. PP composites with PBE concentrations ranging from 0 to 50 wt% were prepared and subjected to cobalt-60 gamma-ray irradiation at doses ranging from 0 to 250 kGy. Electrical properties, including electrical conductivity, trap distribution, and alternating (AC) breakdown strength, were measured. The physical and chemical structures of the samples were estimated. The results indicate that the electrical properties of the irradiated sample increased with the addition of PBE, which is related to the effect on changes in the molecular chain generated by irradiation.

2 Experimental setup

2.1 Sample preparation

Isotactic PP (iPP) served as the base material, and PBE, with a molecular chain composition of 85 wt% propylene and 15 wt% ethylene, functioned as a modifier. The sample was prepared using iPP and PBE with varying content (10–50 wt%) in an internal mixer at 170 °C for 6.5 m at 60 r/min. This ensured sufficient blending and optimal performance. The hot-press method was employed to create the test samples 185 °C at a pressure of 16 MPa for 10 min. The resulting square samples measured 9 cm on each side and had a thickness of 0.15 mm. To investigate the alterations in the electrical performance and microstructures under irradiation, the samples were subjected to cobalt-60 gamma-ray irradiation by BFT-IV at a dose rate of approximately 3 kGy/h. To capture the substantial variations in electrical performance with irradiation, a reference was made to the actual operating conditions of NPPs, and irradiation doses of 80 kGy and 250 kGy were selected to represent the states of mild and severe aging [5, 21]. For convenience, the sample names are distinguished in the following sections. For example, "PB30-250" designated a sample containing 30 wt% PBE subjected to irradiation with 250 kGy.

2.2 Electrical properties

The conduction current, measured using a Picoammeter (B2981A, Keysight, USA) in a three-electrode system, recorded data at 1-s intervals. Furthermore, an electrode with a diameter of 3.5 cm maintains a gap of 2 mm from the ground electrode. At an applied field strength of 20 kV/mm, current data were recorded over 2000s. The current was determined by averaging the data from the last 60 s.

The carrier trap distribution was evaluated via isothermal surface potential decay (ISPD) measurements following the

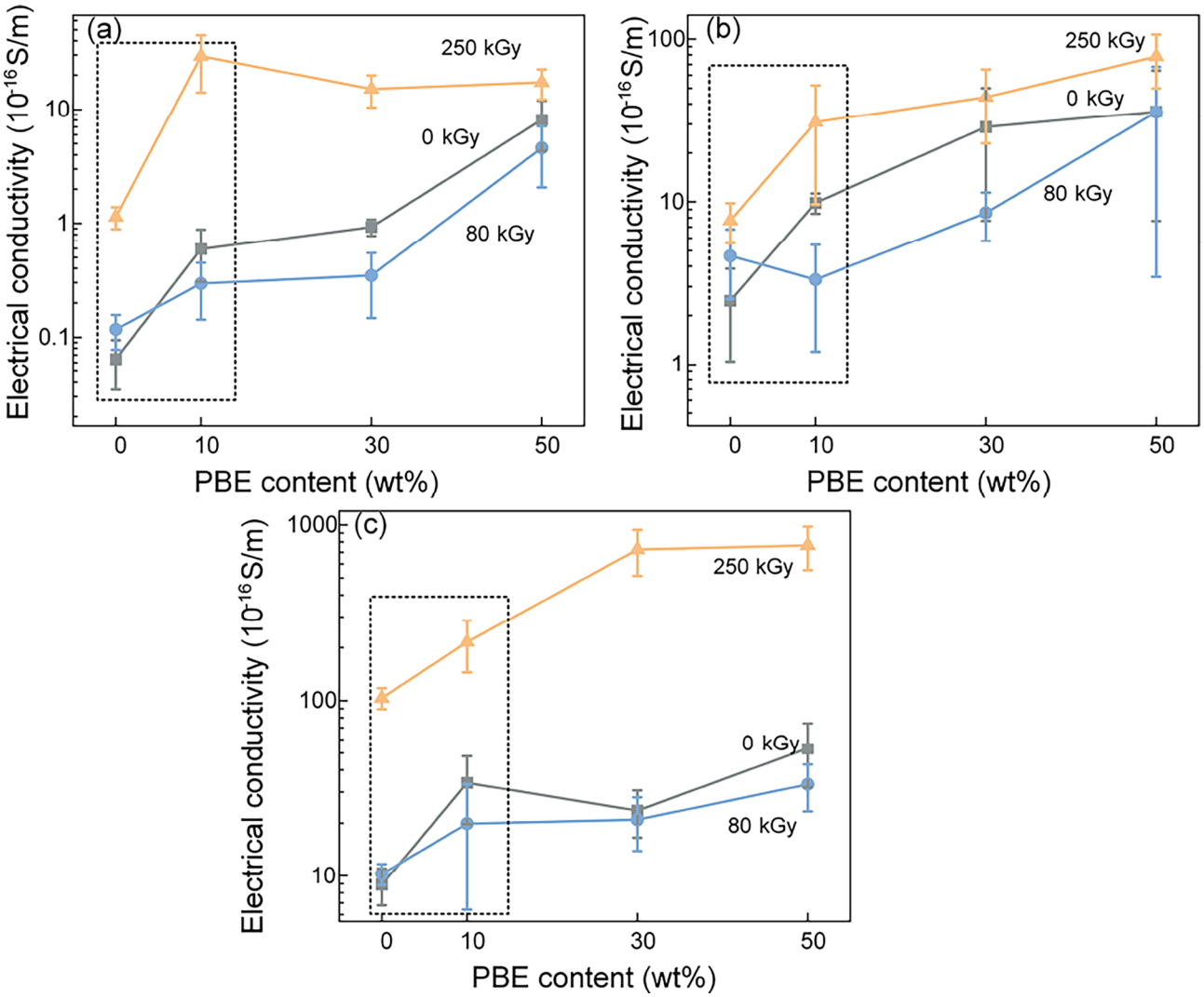

Fig. 1 (Color online) Relation between electrical conductivity and the PBE content of the sample at different total doses and temperatures **a** 30 °C, **b** 50 °C, and **c** 70 °C

detailed procedure and calculation method from our previous publication [25]. The needle and grid electrodes were set to –6.5 kV and –3.0 kV, respectively, with a 15-min charging time. Testing occurred at 40 °C with a relative humidity of 20%± 5%. The average results from at least three samples are presented.

AC breakdown strength is one of the most important indicators of insulation performance. The measurements were taken using two hemispherical brass electrodes. Specifically, one electrode was connected to an AC power source (Wuhan Sanxin Huatai Electrical Testing Equipment Co., Ltd., China) and the other electrode was grounded. During the tests, the AC voltage increased at a rate of 0.5 kV/s until a breakdown path was formed in the sample. Data from multiple trials were recorded and analyzed using the Weibull distribution [26].

2.3 Physical and chemical structures

The crystallization and melting behaviors of the sample were evaluated via differential scanning calorimetry (DSC) measurement (Netzsch DSC 200 F3) under a temperature range of 30 °C to 200 °C in a nitrogen atmosphere, with a heating/cooling rate of 10 °C/min. Fourier transform infrared spectroscopy (FTIR) (Agilent Cary 630 FTIR spectrometer) was conducted in the wavenumber range of 400 cm^{-1} to 4000 cm^{-1}, with a resolution of 2 cm^{-1}. Thermogravimetric analysis (TGA) was conducted (using a TAQ500 instrument) to measure the sample mass variation with temperature, which ranged from 30 to 600 °C in a nitrogen atmosphere with a nitrogen gas flow rate of 60 mL/min and a heating rate of 20 °C/min. The microscopic morphology was estimated using Scanning Electron Microscopy (SEM) with an

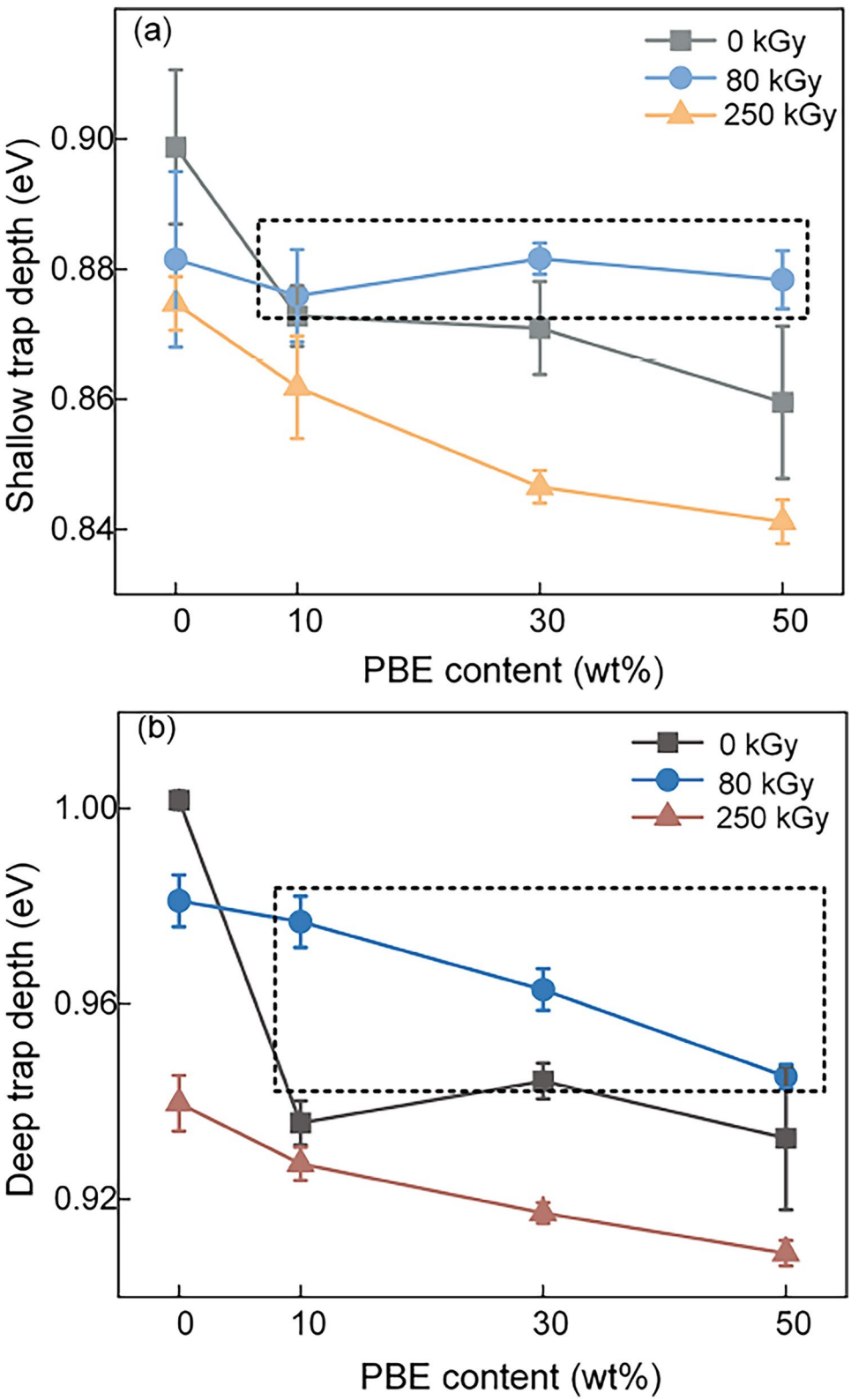

Fig. 2 (Color online) Relation between the trap depth and PBE content for the sample with various total doses. **a** Shallow trap depth and **b** deep trap depth

FEI Nanosem430. High-temperature gel permeation chromatography was used to measure the molecular weights of the polymers. Furthermore, PL EasiCal PS-1 was used as the standard sample, the test temperature was 150 °C, and 1,2,4-trichlorobenzene (TCB) was used as the mobile phase. Furthermore, 0.05 wt% 2,6-di-tert-butyl-4-methylphenol (BHT) was added to the solvent as an antioxidant. More

detailed information about the experiment was reported in our previous study [21].

It should be noted that the GPC results only show the molecular weight (M_w) of the polymer with linear structures that can be dissolved in the solvent. It was determined that all unirradiated and iPP samples can be dissolved in xylene at 150 °C. However, some parts of the irradiated blend sample cannot be dissolved, indicating that crosslinked bonds appeared in the irradiated blends. In this study, the crosslinking degree of materials without any crosslinking agent was relatively low, making it difficult to represent it using conventional measurement methods. Furthermore, SEM was used to more intuitively demonstrate the crosslinking effect of irradiation on the sample. The PBE was dissolved in xylene, whereas iPP and its crosslinked structures were insoluble in xylene at room temperature. Hence, when the sample was immersed in xylene for 3 h at room temperature, the linear elastomers were dissolved, and other parts were left to be observed. The microstructure changes in the sample subjected to irradiation were analyzed.

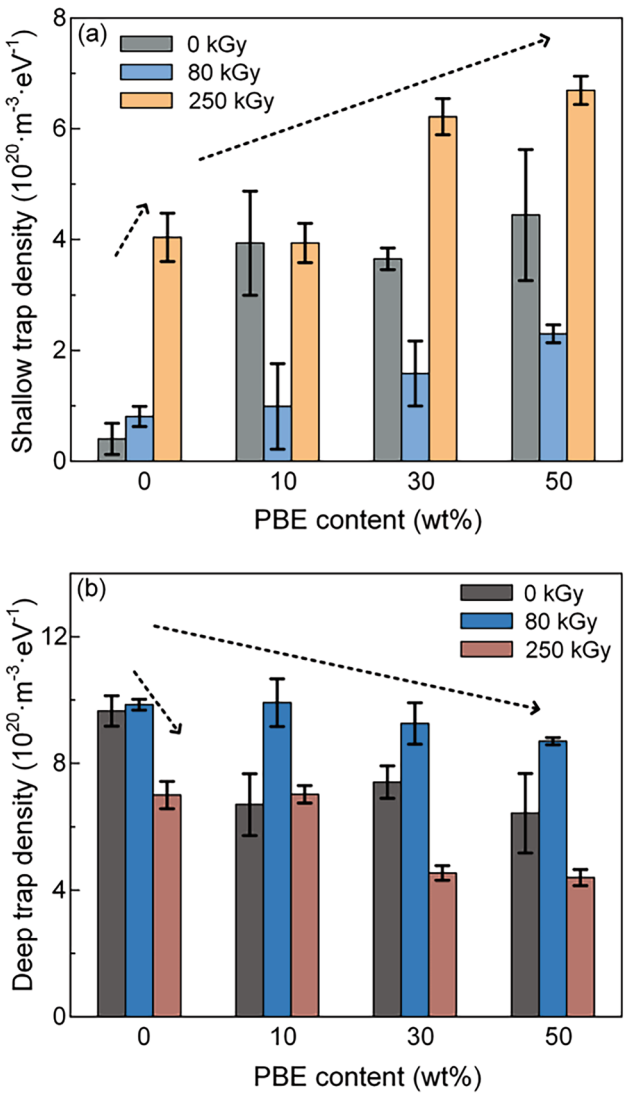

Fig. 3 (Color online) Relation between the trap density and PBE content for the sample with various total doses. **a** Shallow trap density and **b** deep trap density

3 Results

3.1 Electrical conductivity

Generally, polymeric materials exhibit low electrical conductivity; however, their electrical conductivity increases with irradiation-induced degradation. Electrical conductivity was measured to understand the impact of irradiation on the sample. During testing, the charging current experienced a rapid initial decline, with the descent rate slowing over time, signifying a transition from transient-dominated to conduction-dominated current [27]. Figure 1 depicts the relationship between the electrical conductivity and PBE content of the sample at different total doses and temperatures. This is shown in Fig. 1a. As the PBE content increases, the electrical conductivity increases. The electrical conductivities of the samples with various PBE contents exhibited varying changes after irradiation. With an increase in the total dose, the electrical conductivity decreases first and then increases for the iPP/PBE blend sample. This is distinct from the electrical conductivity of the sample without PBE, which continuously increases with irradiation. It was observed that the electrical conductivity of pure iPP was the lowest for the unirradiated sample. However, for the iPP/PBE blend sample, the electrical conductivity was the lowest for the sample irradiated with 80 kGy, which is in the range of 10^{-16}–10^{-17} S/m. This implies that the conductivity of the blend sample decreases owing to the irradiation. The electrical conductivity of the sample irradiated with 250 kGy is an order of magnitude higher than that of the other samples, indicating that deterioration in performance from high-dose irradiation is difficult to avoid. For the samples irradiated at the same total dose, the electrical conductivity increased with increasing PBE content. The variations in electrical conductivity with the PBE content and total doses were similar at temperatures of 30, 50, and 70 °C. Electrical conductivity increased with temperature. Additionally, the electrical conductivity increased with increasing PBE content at all temperatures. However, this increase in electrical conductivity decreased with increasing temperature.

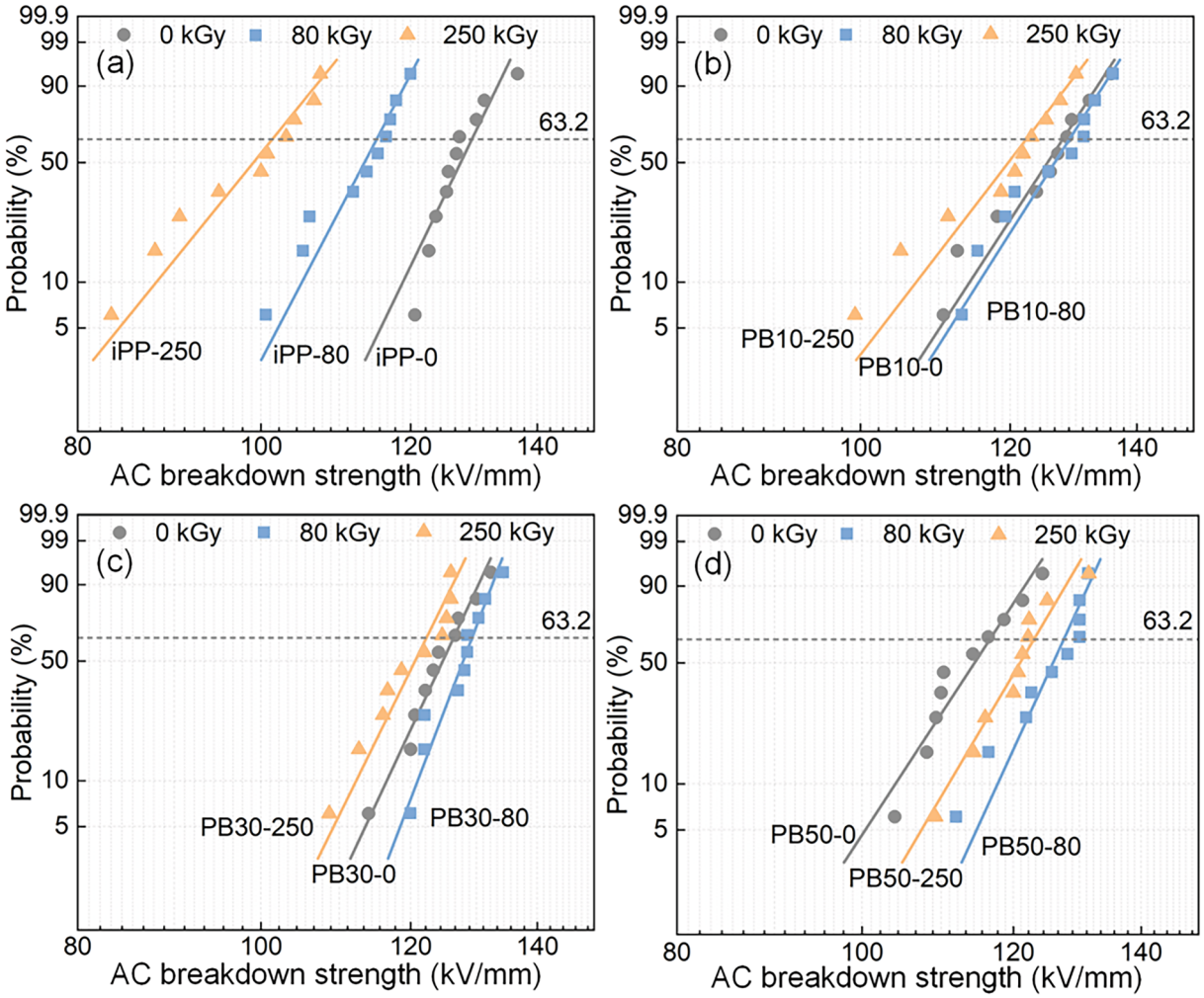

Fig. 4 (Color online) Weibull distribution images of the AC breakdown strength for sample **a** iPP, **b** PB10, **c** PB30, and **d** PB50

Table 1 AC breakdown parameters of the sample with different PBE contents and total doses

Sample	E (kV/mm)	Shape
iPP-0	129.27	26.79
PB10-0	127.91	19.85
PB30-0	126.41	27.69
PB50-0	116.62	19.77
iPP-80	115.12	24.74
PB10-80	128.97	20.37
PB30-80	129.29	34.01
PB50-80	127.52	28.24
iPP-250	101.39	15.92
PB10-250	122.36	16.79
PB30-250	122.31	26.28
PB50-250	122.98	21.91

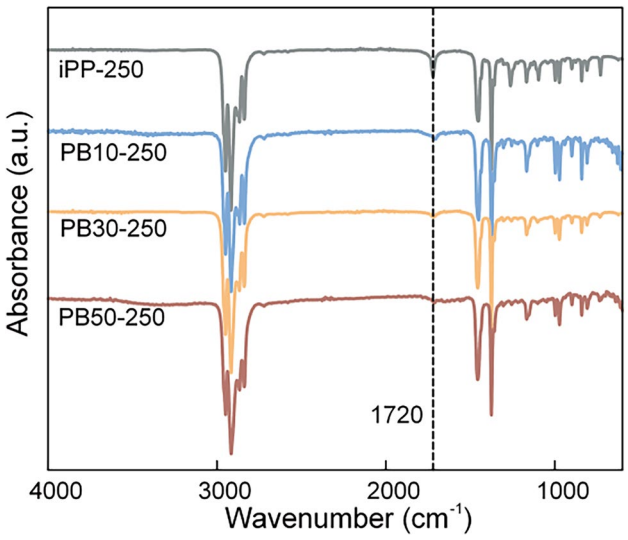

Fig. 5 (Color online) FTIR of different samples irradiated with 250 kGy

3.2 Trap distribution

Carrier traps are formed by physical or chemical defects in materials and play an important role in the charge transport behavior, which can aid in understanding the changes in the electrical properties of insulation materials [28]. Figure 2 shows the relationship between the trap depth and PBE content of the sample irradiated with various total doses. As the PBE content increases, the depths of the deep and shallow traps decrease for most samples. For unirradiated samples, despite the introduction of PBE elastomers (10 wt %), the trap depth exhibited an acute drop. With the introduction of PBE elastomers, the decline in trap depth slowed. For shallow traps, the trap depth of iPP-0 was the deepest, and the trap depths of PB10-0 and PB30-0 were similar. However, the trap depth of PB50-0 was much lower than that of the others. For the deep traps, the depth of the iPP/PBE blend sample was approximately 0.94 eV and that of iPP was 1.01 eV. This shows that PBE elastomers have a strong impact on the trap depth; however, this impact decreases with increasing irradiation dose. The difference in trap depth between iPP and PB10 was less obvious at 80 and 250 kGy. For the irradiated samples, as the PBE content increased, the depths of both traps decreased. Notably, the shallow trap

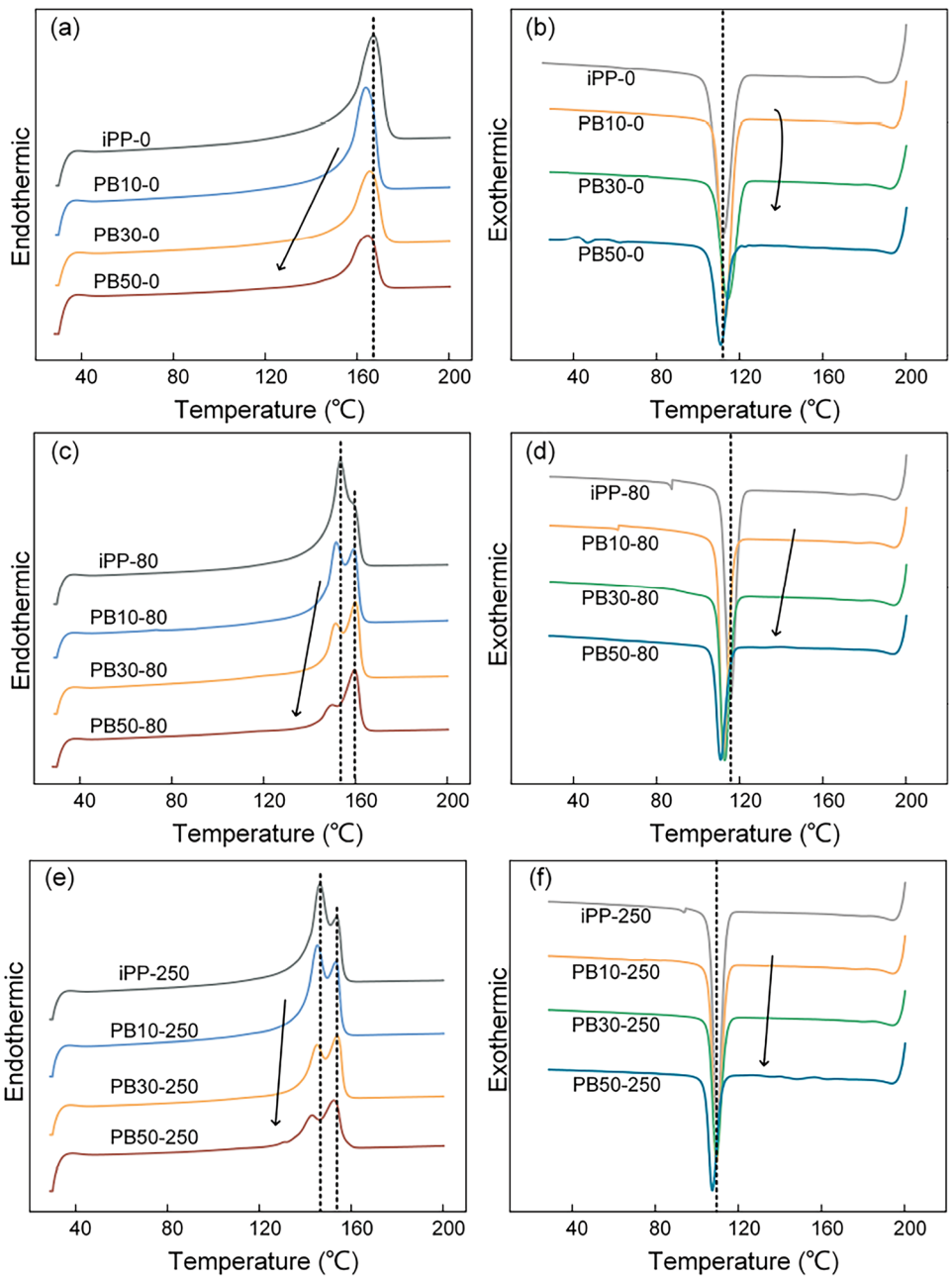

Fig. 6 (Color online) Variation in melting and crystallization curves for the sample with different total doses. **a** Melting and **b** crystallization curves for the sample with 0 kGy. **c** Melting and **d** crystallization curves for the sample with 80 kGy. **e** Melting and **f** crystallization curves for the sample with 250 kGy

depths are approximately 0.88 eV for all samples with various PBE contents at 80 kGy. As the total dose increased, the alternations in the trap depth exhibited different trends for pure iPP and iPP/PBE blend samples. The trap depth of iPP continuously decreased with the total dose. For the iPP/PBE blend sample, the trap depths at 80 kGy are greater than those at 0 kGy. This indicated that the trap depth of the blended sample initially increased and then decreased as the total dose increased from 0 to 250 kGy. Additionally, the error bar is obvious for unirradiated samples, especially for the sample with a higher PBE content. However, the error bar becomes less pronounced as the irradiation dose increases. Hence, it can be inferred that the performance of the blended sample may stabilize with the irradiation dose.

The relationship between the density of shallow traps and PBE content for samples irradiated with various doses is shown in Fig. 3a. For shallow traps, as the PBE content expands from 0 wt% to 10 wt%, the trap density increases sharply, and its growth is more than 3×10^{20} $m^{-3} \cdot eV^{-1}$. Subsequently, with the PBE content increasing from 10 wt% to 50 wt%, the trap density emanates almost no change, all around 4×10^{20} $m^{-3} \cdot eV^{-1}$. As the irradiation increases, the changes in the trap density of iPP and iPP/PBE blend samples differ. It can be observed that the shallow trap density declines at the irradiation stage, from 0 to 80 kGy, and increases at the stage from 80 to 250 kGy for the blend samples. However, those two stages for iPP samples display an increase. The changes in the deep trap density of the sample are opposite to those of the shallow traps, as shown in Fig. 3b. The deep trap density decreases with increasing PBE content. The unirradiated iPP and sample irradiated with 80 kGy exhibit the deepest trap depths.

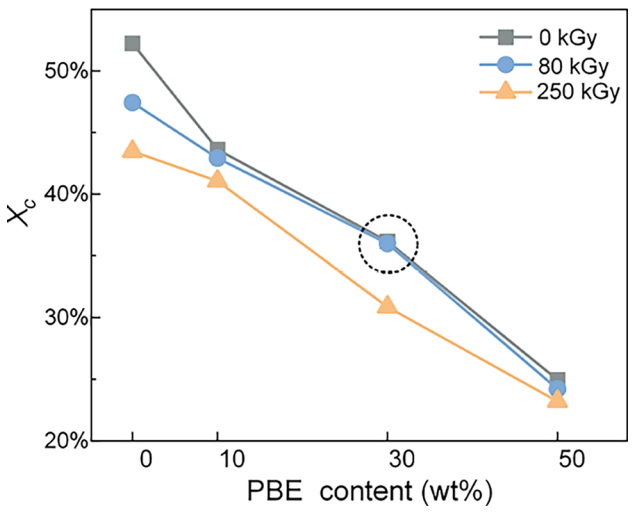

Fig. 7 (Color online) Changes in X_c of samples with different total doses

3.3 AC breakdown strength

Cables in NPPs operate under AC electric fields. Thus, AC breakdown strength is one of the most important parameters for evaluating the performance of insulation materials in NPPs. The AC breakdown strength distributions of samples with different PBE contents are shown in Fig. 4, which exhibit quite different trends with increasing irradiation. For iPP samples, the breakdown strength showed an apparent downswing, suggesting that it was sensitive to gamma-ray irradiation. However, for all the blend samples, the breakdown strength initially increased and then decreased, indicating that irradiation can improve the breakdown strength of the blend sample at low total doses. Specifically, after irradiation at 250 kGy, the breakdown strength of PB50 was significantly higher than that of the initial sample.

To accurately analyze the breakdown performance of the sample, the breakdown parameters are extracted and are listed in Table 1. Specifically, E denotes the breakdown strength with a cumulative failure probability of 63.2%. The shape parameter reflects the dispersion of the data. The higher the shape parameter, the lower is the dispersion of the breakdown strength. As the PBE content increased from 0 to 30 wt%, E decreased marginally; however, when the PBE content increased to 50 wt%, E decreased dramatically. When the total dose was increased, E of the blend sample showed an evident improvement when compared to iPP. The E value of PB30-80 was 14.17 kV/mm higher than that of iPP-80, indicating that the addition of the PBE elastomer increased the breakdown strength under irradiation. At 250 kGy, this improvement was more apparent, for which the E values of all the blends were 21% higher than that of iPP. It can be inferred that the addition of PBE elastomer can improve the irradiation resistance of iPP. This improvement was stable, as confirmed by the shape parameter values.

3.4 Physical and chemical structures

The oxidation of the sample reflects the aging conditions of the polymer. The peak at 1720 cm^{-1} corresponds to the carbonyl group, the intensity of which can be used to distinguish the degree of oxidation of the polymer materials [29]. It has been reported that the intensity of the carbonyl peak increases with the total dose and that the carbonyl peak is not obvious in the unirradiated sample [21]. To more clearly observe the oxidation of the sample under irradiation, Fig. 5 shows the FTIR spectrum of the sample irradiated at 250 kGy. As the PBE content increased, the intensity of the carbonyl peak decreased, suggesting that the addition of the PBE elastomer was beneficial for preventing oxidation reactions, thereby increasing the irradiation resistance.

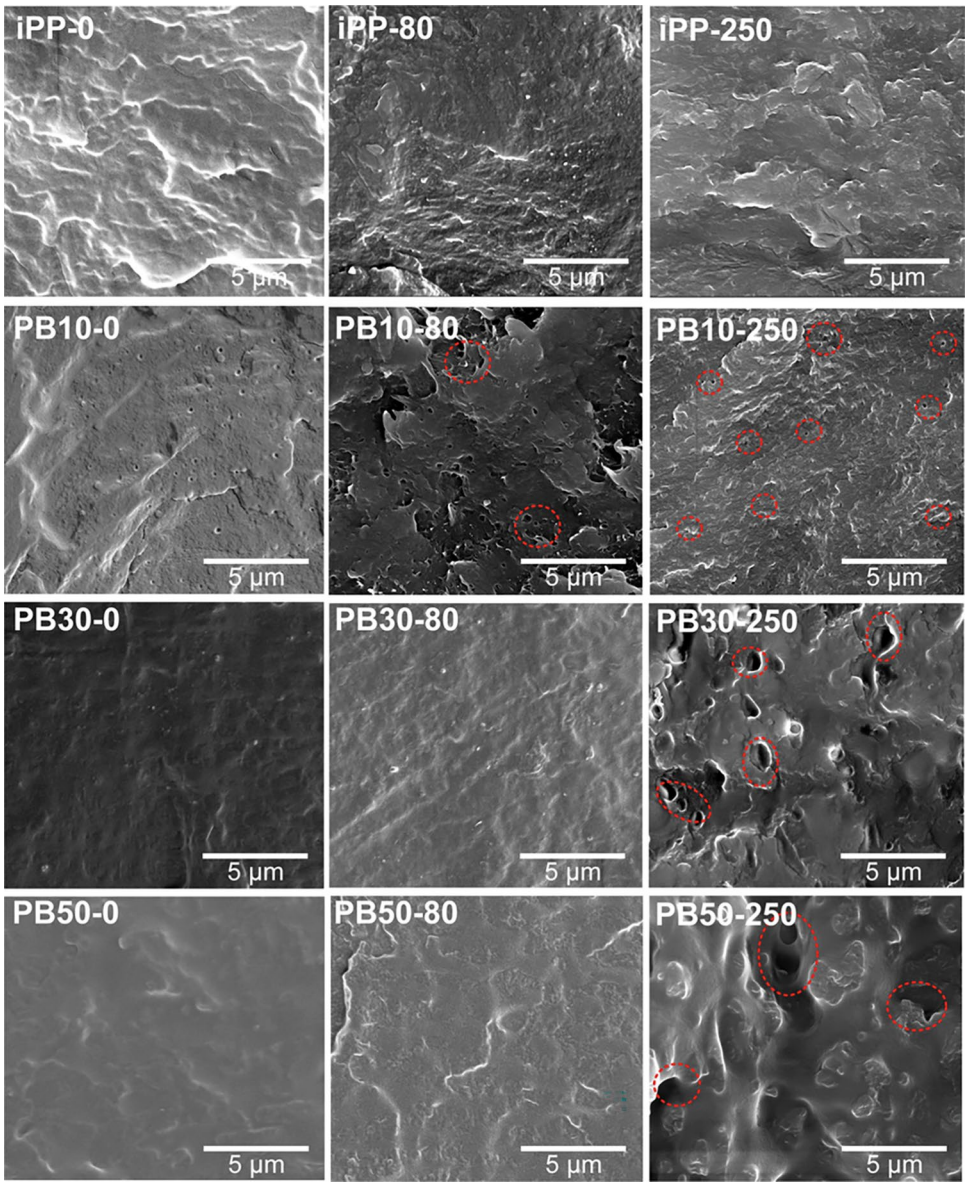

Fig. 8 (Color online) Micromorphology photographs of the samples with different PBE contents and total doses

The melting and crystallization curves of the samples reflect variations in the physical and chemical structures. In Fig. 6a, for unirradiated samples, as the PBE content increases, the melting peak shifts to the left, indicating that the introduction of PBE elastomer decreases the melting point (T_m). In Fig. 6b, the variation in the crystallization curves is not obvious. As the total dose increases, from 0 kGy to 80 kGy, the melting peaks change from one to two for all samples, as shown in Fig. 6c. This indicated that components with different T_m appear after irradiation. The melting peak decreased with increasing PBE content. The crystallization temperature (T_c) decreases with increasing PBE content at 80 kGy. Similar phenomena were observed at 250 kGy. The T_m and T_c values of the irradiated samples showed only slight changes with the PBE content. The T_c values of all samples were approximately 110 °C. Nevertheless, the difference in melting behavior induced by irradiation was exaggerated. As the total dose increased, T_m decreased from 164 to 153 °C for all samples, and the separation of the melting peaks became increasingly apparent. In particular, the separated melting peak located on the left became more prominent with increasing total dose, which was attributed to the component with a lower T_m increase. The crystallinity (X_c) was derived from the melting curves as shown in Fig. 7. As the PBE content increased, X_c decreased significantly. The X_c of PB10-0 was 43%, a decline of 9% when compared to iPP-0. The X_c of iPP decreased constantly with the total dose; however, the X_c of the blend exhibited almost no change with irradiation from 0 to 80 kGy. As the total dose increased to 250 kGy, slip occurred in all samples.

The micromorphology of polymers may undergo severe changes upon gamma-ray irradiation, particularly for

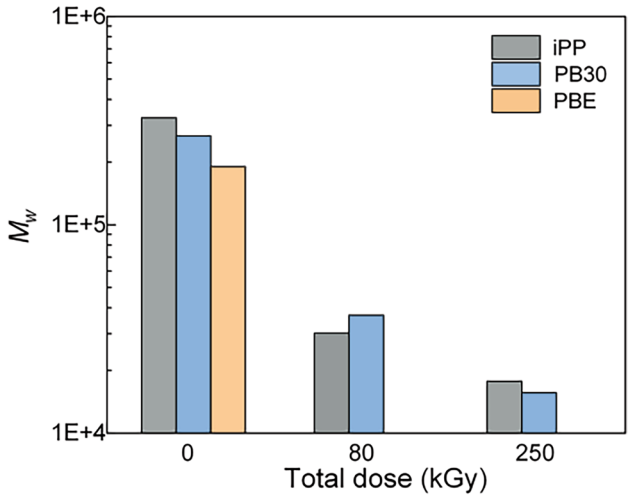

Fig. 9 (Color online) GPC results of iPP and PB30 with different total doses

polymers with more than one component. The morphologies of the iPP samples were similar at different total doses and were smooth and uniform (Fig. 8).

The morphology of the cross section of iPP/PBE blend samples with different total doses exhibited certain discrepancies. For the unirradiated blend sample, no obvious defects appeared in the cross section, implying that the blending was uniform. As the total dose increased, defects gradually appeared in all blend samples, indicating the phase separation of PBE and iPP. It can be observed that high numbers of pores and wrinkles occur in the cross section, parts of which are marked by red dashed circles. For PB10, the number of pores increased with increasing irradiation, but their size decreased. As the PBE content increased to 30 and 50 wt%, no phase separation occurred at low total doses, whereas the defects in the sample irradiated with 250 kGy were conspicuous. This indicates that deterioration in the combination of the two phases occurs during irradiation from 80 to 250 kGy.

The M_w value of a polymer is uneven and is a critical factor in its electrical performance. Figure 9 illustrates the weight-average M_w of iPP and PB30 with different total doses, which is the result of the GPC. As the cumulative dose increased, the M_w of the sample exhibited an intense decrease. The difference between the M_w of iPP and PB30 was not significant at the same total dose. The M_w of PB30-0 was lower than iPP-0, but the M_w of PB30-80 was higher than iPP-80, suggesting that the degree of damage due to irradiation varied with the molecular chains of the different polymers. SEM images of the cross section of the sample immersed in xylene are presented in Fig. 10. The microscopic morphology images of PB30-0 and PB30-250 after treatment show the influence of irradiation at 250 kGy. There were many large pores or gullies in PB30-0 treated with xylene, whereas those in PB30-250 treated with the xylene treatment were less significant (marked by yellow dashed rectangles). This indicates that a denser crosslinked structure was formed, which was insoluble in xylene and could be generated via irradiation.

The thermal decomposition temperature provides insight into the thermal stability of the sample. The temperatures at mass losses of 5% and 50% are defined as the thermal decomposition temperatures T_5 and T_{50}, respectively. The thermogravimetric curves of PB30 are shown in Fig. 11a, which shows that T_5 and T_{50} slip sharply with the cumulative dose. The decline between PB30-80 and PB30-0 in T_5 is approximately 80 °C, indicating that the thermal stability of the sample slips sharply upon irradiation. Figure 11b illustrates the thermogravimetric curves of samples with different PBE contents irradiated with 250 kGy. As the PBE content increases, T_5 and T_{50} values of all the samples almost overlap. Obviously, the thermal stability of the sample was not affected by the addition of PBE elastomer at 250 kGy, whereas it was significantly reduced by irradiation.

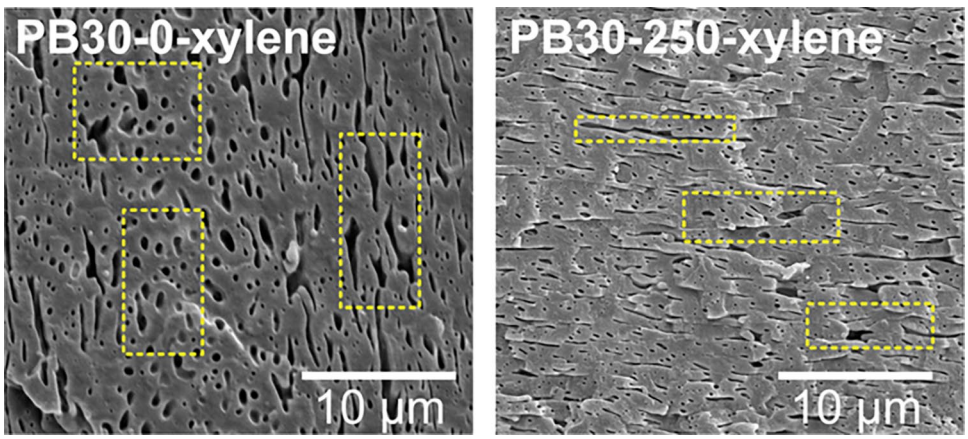

Fig. 10 (Color online) SEM images of PB30-0 and PB30-250 treated with xylene

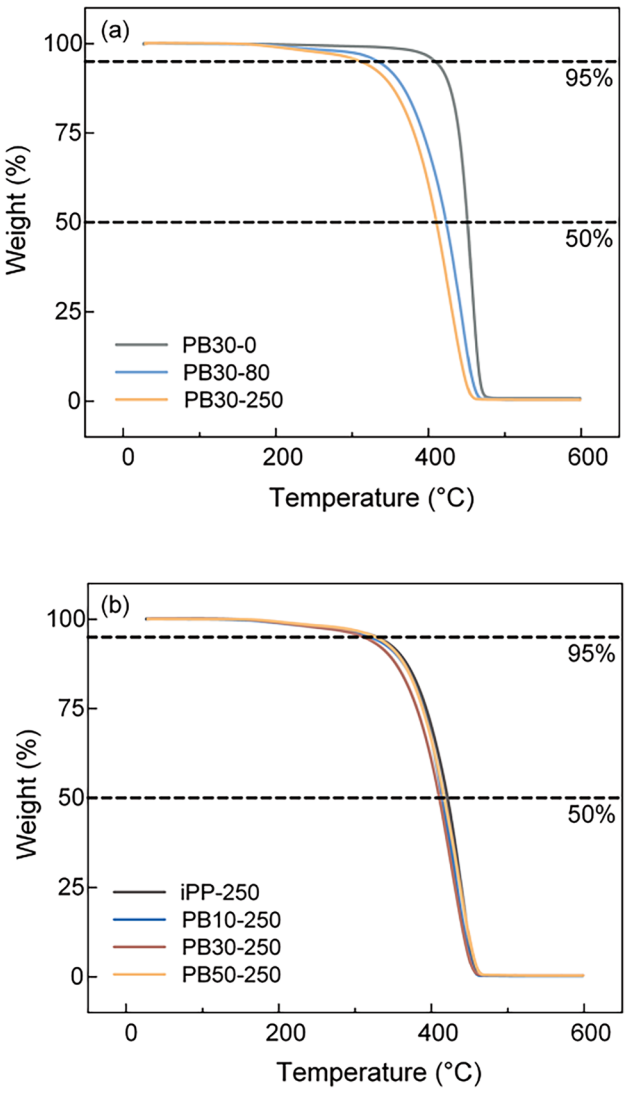

Fig. 11 (Color online) Thermogravimetric curve of the sample. **a** PB30 with different total doses and **b** samples with different PBE contents irradiated by 250 kGy

4 Discussion

As mentioned above, when compared with the iPP sample, the iPP/PBE sample exhibited a higher breakdown strength and lower conductivity after irradiation. The addition of the PBE changed the physical and chemical structures of the iPP matrix, leading to improved electrical properties after irradiation. To visually describe the effect and mechanism of irradiation on the samples, a schematic based on the aforementioned experimental results is shown in Fig. 12. It is essential to elucidate the degradation mechanism of iPP before investigating the mechanism of the improvement introduced by PBE under irradiation. As shown in Figs. 12a and (b), unirradiated iPP with higher X_c and fewer amorphous regions can be obtained from the DSC results. Hence, this leads to extremely high regularity of the molecular chains, resulting in more carrier trap centers and deeper traps, as shown in Figs. 2 and 3 [30, 31]. The carrier traps of insulation materials can capture carrier charges and hinder the transport of carriers. Therefore, it differs to form a charge transport path for unirradiated iPP, leading to better insulation properties when compared to the other samples.

This changes after irradiation as shown in Figs. 12c and d. High-energy irradiation damages the polymer molecular chains [30–33]. There are a large number of tertiary carbon atoms in the molecular chains of iPP, which have low bond energies and are easy to break. Therefore, iPP is sensitive to irradiation [13, 30]. The results of DSC, GPC, and TGA show a shortage of molecular chains in the sample with the total dose, indicating that massive chain scission occurred. Many broken bonds appear in the irradiated iPP; then, the low-density region can be generated, which is the result of the accumulation of damage in molecular chains [33, 34]. The AC breakdown path of the insulation materials may initially be induced in the low-density region (indicated by the purple dashed arrow lines). Meanwhile, polar groups are introduced into the molecular chain because of irradiation-induced oxidation, which decreases X_c and increases the amorphous regions and free volume of the sample, as shown in Figs. 5, 6, 7. The depth and density of the traps are reduced owing to more broken bonds and amorphous regions with irradiation, leading to a shallower depth and lower density of traps, as shown in Figs. 2 and 3. Charge transport is promoted, electrical conductivity increases, and the breakdown strength decreases.

The improvement in the electrical performance of iPP under irradiation environment is closely related to its molecular chain structure, as shown in Figs. 12e–h. It should be noted that the impact of irradiation and electrical properties is material-dependent [21, 35]. The structural alteration in the blend samples with irradiation was distinct from that in the iPP samples, which was the reason for the improved electrical properties with increasing total dose. As the PBE content increases, the electrical properties of the non-irradiated samples decrease, as shown in Figs. 1, 2, 3, 4. This is because the addition of PBE decreases the regularity of the sample, X_c decreases, and the amorphous regions increase, as shown in the DSC results. However, after irradiation, the sample with the highest PBE content exhibited better electrical properties, suggesting that it had better irradiation resistance. For PBE, there is some ethylene in the molecular chains, which results in fewer tertiary carbon atoms and more secondary carbon atoms when compared with those of iPP, which has a higher bond energy. Therefore, it is less susceptible to breakage under irradiation [21, 30]. As the PBE content increased, the negative impact of irradiation on the molecular structure decreased, which assisted the sample in maintaining better performance. Moreover,

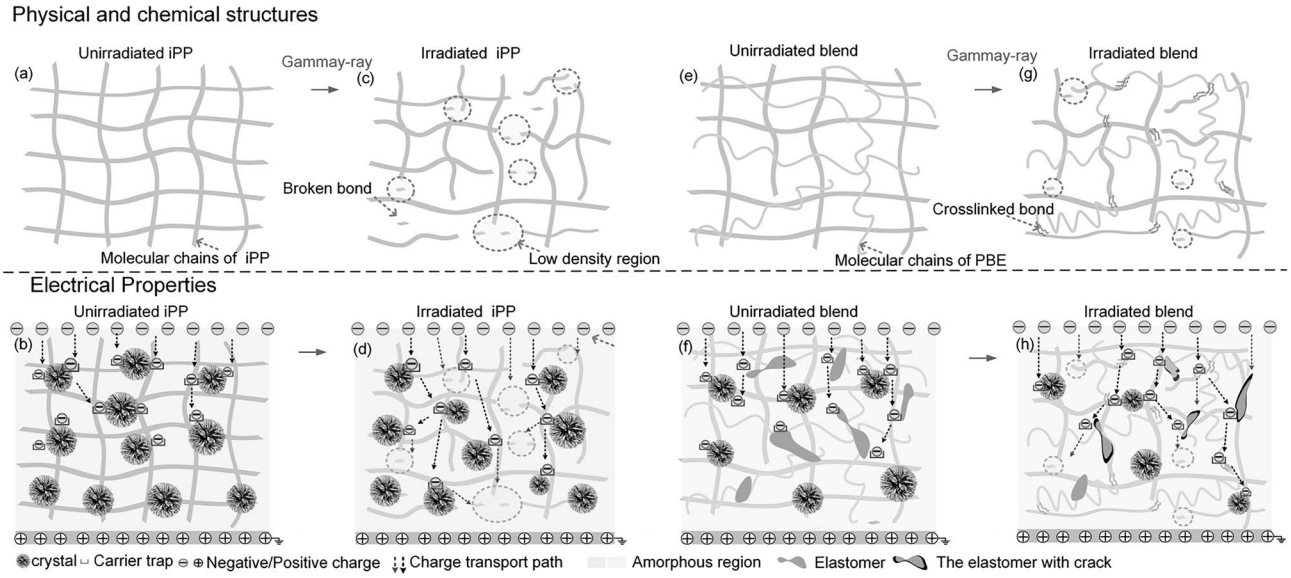

Fig. 12 (Color online) Improvement mechanism of PBE on the electrical properties of iPP under irradiation. **a** Structures and **b** electrical properties for unirradiated iPP samples. **c** Structures and **d** electrical properties for irradiated iPP samples. **e** Structures and (f) electrical properties for unirradiated blend samples. **g** Structures and **h** electrical properties for irradiated blend samples

when the total dose is increased, crosslinking occurs, as shown in Fig. 10, which arranges the molecular chains in a more compact manner. Crosslinking bonds interconnect the molecular chains, resulting in the formation of a dense structure that minimizes the presence of short chains and decreases the number of low-density regions. The dense configuration restricts the permeation of oxygen, consequently mitigating the oxidation processes. The carrier trap of the blended sample deepens, as shown in Figs. 2 and 3, which may also be attributed to the crosslinked bonds. These factors are beneficial for improving the electrical properties. It has been revealed that denser structures of molecular chains provide materials with distinct performances, including high antioxidant capacities [34]. Therefore, irradiation-induced crosslinking not only reduces the number of broken bonds but also increases the antioxidant capacity, all of which are beneficial for the irradiation resistance of the sample. The crosslinked structure is also beneficial for improving the performance of materials at higher temperatures [36–38]. Consequently, the improvement in the electrical performance of the sample is reasonable. However, as a mixture with two-phase structures, the compatibility between iPP and PBE significantly affected the performance of the blended sample. When the compatibility decreases with increasing dose, defects occur at the point of phase separation, seriously degrading the electrical properties, as shown in Fig. 8. This was the main reason for the decrease In the performance of the blend sample irradiated with a total dose of 250 kGy.

5 Conclusion

In this study, the electrical properties of an iPP/PBE blend under gamma-ray irradiation were investigated, yielding the following main findings:

1. The addition of PBE led to an overall increase in electrical conductivity. For the iPP samples, electrical conductivity consistently increased as the total dose increased from 0 kGy to 250 kGy. For the blended sample, the electrical conductivity initially decreased and then increased with cumulative dose.
2. With increasing irradiation, the trap distribution in the iPP sample tends to become shallower, whereas in the blended sample, it initially deepens to 80 kGy before shallowing. Unirradiated samples showed shallower trap distributions with a higher PBE content.
3. The incorporation of PBE notably enhanced the AC breakdown strength of the irradiated sample by more than 21% when compared with iPP at 250 kGy. The breakdown strengths of the iPP samples decreased significantly after irradiation. The breakdown strength of the blend increased with the cumulative dose up to 80 kGy and then decreased, with a more pronounced improvement at higher PBE contents.
4. Increasing PBE content was correlated with a decrease in the intensity of the carbonyl peak at 250 kGy. The microscopic morphologies of the blended samples retained their original form at lower doses but exhibited

phase separation at higher doses. The addition of PBE mitigated the damage to the molecular chains of iPP and promoted the formation of crosslinked structures.

In summary, this study revealed that the electrical properties of irradiated iPP can be improved by introducing PBE. The deterioration of electrical properties is linked to the molecular chain structure, including M_w, X_c, and oxidation. The iPP/PBE blend sample demonstrated a higher breakdown strength than the irradiated iPP, which is attributed to the enhanced irradiation resistance and formation of crosslinked structures. These findings suggest a promising choice of cable insulation materials for NPPs, contributing to their safe operation.

Author contributions All authors contributed to the study conception and design. Material preparation, data collection, and analysis were performed by Bai-Xin Liu, Yu Gao, Jing Li, Chen-Yi Guo, Bo-Sen Si, Jun-Guo Gao, Yu Chen, and Bo-Xue Du. The first draft of the manuscript was written by Bai-Xin Liu, and all authors commented on previous versions of the manuscript. All authors read and approved the final manuscript.

Data availability statement The data that support the findings of this study are openly available in Science Data Bank at https://cstr.cn/31253.11.sciencedb.j00186.00290 and https://www.doi.org/10.57760/sciencedb.j00186.00290.

Declarations

Conflict of interest The authors declare that they have no conflict of interest.

References

1. C. Li, Y. Yang, G. Xu et al., Insulating materials for realising carbon neutrality: opportunities, remaining issues and challenges. High Volt. **7**, 610–632 (2022). https://doi.org/10.1049/hve2.12232
2. Y. Zhou, P. Hao, X. Zhang et al., Numerical investigations of thermal mixing performance of a hot gas mixing structure in high-temperature gas-cooled reactor. Nucl. Sci. Tech. **27**, 23 (2016). https://doi.org/10.1007/s41365-016-0024-7
3. Z. Zhang, Y. Dong, Q. Shi et al., 600-MWe high-temperature gas-cooled reactor nuclear power plant HTR-PM600. Nucl. Sci. Tech. **33**, 101 (2022). https://doi.org/10.1007/s41365-022-01089-9
4. S. Jiang, J. Tu, X. Yang et al., A review of pebble flow study for pebble bed high temperature gas-cooled reactor. Exp. Comput. Multiph. Flow. **1**, 159–176 (2019). https://doi.org/10.1007/s42757-553019-0006-1
5. Y. Gao, B. Liu, B. Du et al., Research progress and prospect of cable insulation in nuclear power plants. High Volt. in China. **48**, 78 (2012). https://doi.org/10.1140/epja/i2012-12078-5
6. X. Shen, J. Wu, W. Li et al., Effects of electric field and temperature on charge transport in an LDPE/SiO_2 nanocomposite. IEEE Trans. Dielectr. Electr. Insul. **30**, 2532–2542 (2023). https://doi.org/10.1109/TDEI.2023.3303858
7. J. Li, C. Zhang, T. Chen et al., Irradiation and flame retardant effect of poly[bis(phenoxyphosphazene)] and magnesium hydroxide in LDPE composites. Nucl. Sci. Tech. **26**, 030304 (2015). https://doi.org/10.13538/j.1001-8042/nst.26.030304
8. Y. Gao, X. Feng, L. Li et al., Preparation of a starch-based superabsorbent polymer by gamma-ray irradiation and investigation of its properties. J. Radiat. Res. **41**, 010204 (2023). https://doi.org/10.11889/j.1000-3436.2022-0112
9. K. Yang, Y. Ren, K. Wu et al., Enhancing electrical properties of impact polypropylene copolymer for eco-friendly power cable insulation by manipulating the multiphase structure through molten-state annealing. Compos. Sci. Techno. **223**, 109422 (2022). https://doi.org/10.1016/j.compscitech.2022.109422
10. S. Li, D. Xie, G. Qu et al., Tailoring interfacial compatibility and electrical breakdown properties in polypropylene based composites by surface functionalized POSS. Appl. Surf. Sci. **478**, 451–458 (2019). https://doi.org/10.1016/j.apsusc.2019.01.082
11. S. Cygan, J. Laghari, Effects of fast neutron radiation on polypropylene. IEEE Trans. Nucl. Sci. **36**, 1386–1390 (1989). https://doi.org/10.1109/23.3536
12. S. Cygan, J. Laghari, Dependence of the electric strength on thickness area and volume of polypropylene. IEEE Trans. Dielectr. Electr. Insul. **22**, 835–837 (1987). https://doi.org/10.1140/epja/i2014-14139-1
13. S. Cygan, J. Laghari, Effects of multistress aging (radiation, thermal, electrical) on polypropylene. IEEE Trans. Dielectr. Electr. Insul. **38**, 906–912 (1991). https://doi.org/10.1109/23.81692
14. J.R. Laghari, High-voltage pulsed life for multistressed polypropylene capacitor dielectric. IEEE Trans. Nucl. Sci. **39**, 21–24 (1992). https://doi.org/10.1109/23.120131
15. A. Hammoud, J. Laghari, B. Krishnakumar, Electron radiation effects on the electrical and mechanical properties of polypropylene. IEEE Trans. Nucl. Sci. **34**, 1822–1826 (1987). https://doi.org/10.1109/TNS.1987.4334823
16. N. Yoshiaki, K. Isamu, T. Tohru et al., Radiation-induced conductivity in polymeric insulating materials degraded under specified conditions. IEEE Trans. Dielectr. Electr. Insul. **17**, 306–313 (1982). https://doi.org/10.1109/TEI.1982.298499
17. S. Mouaci, G. Teyssedre, N. Belkahla et al., Charge trapping and conduction in irradiated isotactic polypropylene. IEEE Trans. Dielectr. Electr. Insul. **24**, 3821–3830 (2017). https://doi.org/10.1109/TDEI.2017.006636
18. H. Wang, H. Jiang, R. Shen et al., Electron-beam radiation effects on the structure and properties of polypropylene at low dose rates. Nucl. Sci. Tech. **29**, 87 (2018). https://doi.org/10.1007/s41365-018-0424-y
19. R. Grecco, W. Oliani, D. Parra et al., Accelerated environmental degradation of gamma irradiated polypropylene and thermal analysis. J. Therm. Anal. Calorim. **131**, 823–828 (2018). https://doi.org/10.1007/s10973-017-6653-1
20. T. Oxana, M. Czerny, A. Buettner, Characterisation of flavour compounds formed by gamma-irradiation of polypropylene. J. Polym. Degrad. Stabil. **94**, 757–769 (2009). https://doi.org/10.1016/j.polymdegradstab.2009.02.006
21. B. Liu, Y. Gao, J. Li et al., Ageing behavior of polypropylene as cable insulation under gamma-ray irradiation. IEEE Trans. Dielectr. Electr. Insul. **31**, 956–964 (2024). https://doi.org/10.1109/TDEI.2023.3337753
22. H. Nakatani, S. Suzuki, T. Tanaka et al., New kinetic aspects on the mechanism of thermal oxidative degradation of polypropylenes with various tacticities. Polym. **46**, 12366–12371 (2005). https://doi.org/10.1016/j.polymer.2005.10.131
23. Y. Gao, J. Peng, J. Li et al., Improvement of partial discharge resistance of polypropylene under AC voltage by blending elastomer. IET Sci. Meas. Technol. **17**, 47–57 (2023). https://doi.org/10.1049/smt2.12129
24. Y. Gao, J. Li, G. Chen et al., Compatibility dependent space charge accumulation behavior of polypropylene/elastomer blend

for HVDC cable insulation. IEEE Trans. Dielectr. Electr. Insul. **27**, 947–955 (2020). https://doi.org/10.1109/TDEI.2019.008528
25. Y. Gao, J. Li, Y. Yuan et al., Trap distribution and dielectric breakdown of isotactic polypropylene/propylene based elastomer with improved flexibility for DC cable insulation. IEEE Access. **6**, 58645–58661 (2018). https://doi.org/10.1109/ACCESS.2018.2874826
26. I. Rytöluoto, K. Lahti, M. Karttunen et al., Large-area dielectric breakdown performance of polymer films–part I: measurement method evaluation and statistical considerations on area-dependence. IEEE Trans. Dielectr. Electr. Insul. **22**, 689–700 (2015). https://doi.org/10.1109/TDEI.2015.7076764
27. S. Boggs, D. Damon, J. Hjerrild et al., Effect of insulation properties on the field grading of solid dielectric DC cable. IEEE Trans. Power. Deliver. **16**, 456–461 (2001). https://doi.org/10.1109/61.956720
28. D. Min, H. Cui, Y. Hai et al., Interfacial regions and network dynamics in epoxy/POSS nanocomposites unravelling through their effects on the motion of molecular chains. Compos. Sci. Technol. **199**, 108329 (2020). https://doi.org/10.1016/j.compscitech.2020.108329
29. B. Liu, Y. Gao, Z. Song et al., Thermal cycling induced aging on polypropylene/elastomer blends for DC cable insulation. IEEE Trans. Dielectr. Electr. Insul. **30**, 1802–1809 (2023). https://doi.org/10.1109/TDEI.2023.3236589
30. Z. Pan. Degradation, in *Ploymer Chemistry*, 5th ed. (Chemical Industry Press, China, 2011) 245–257
31. T. Seguchi, K. Tamura, T. Ohshima et al., Degradation mechanisms of cable insulation materials during radiation-thermal ageing in radiation environment. Radiat. Phys. Chem. **80**, 268–273 (2011). https://doi.org/10.1016/j.radphyschem.2010.07.045
32. F. Sha, G. Cheng, Z. Xuan et al., Free-radical evolution and decay in cross-linked polytetrafluoroethylene irradiated by gamma-rays. Nucl. Sci. Tech. **33**, 62 (2022). https://doi.org/10.1007/s41365-022-01039-5
33. Z. Liu, Y. Miyazaki, N. Hirai et al., Comparison of the effects of heat and gamma irradiation on the degradation of cross-linked polyethylene. IEEJ Trans. Electr. Elec. Eng. **15**, 24–29 (2020). https://doi.org/10.1002/tee.23023
34. K. Kao, New theory of electrical discharge and breakdown in low-mobility condensed insulators. J. Appl. Physiol. **55**, 752–755 (1984). https://doi.org/10.1063/1.333133
35. Y. An, Z. Zhang, Y. Wang et al., Structure and properties of high melt strength polypropylene prepared by combined method of blending and crosslinking. J Appl. Polym. Sci. **116**, 1739–1746 (2010). https://doi.org/10.1002/app.31610
36. H. Peng, M. Lu, F. Lv et al., Understanding the effect of silane crosslinking reaction on the properties of PP/POE blends. Polym. Bull. **76**, 6413–6428 (2019). https://doi.org/10.1007/s00289-019-02724-z
37. X. Wen, Z. Li, C. Yang et al., Electron beam irradiation assisted preparation of UHMWPE fiber with 3D cross-linked structure and outstanding creep resistance. Rad. Phys. Chem. **199**, 110370 (2022). https://doi.org/10.1016/j.radphyschem.2022.110370
38. X. Xu, X. Ding, J. Ao et al., Preparation of amidoxime-based PE/PP fibers for extraction of uranium from aqueous solution. Nucl. Sci. Tech. **30**, 20 (2019). https://doi.org/10.1007/s41365-019-0543-05